This is an open access article published under an ACS AuthorChoice License, which permits copying and redistribution of the article or any adaptations for non-commercial purposes.

ACS central science

Research Article

Cite This: ACS Cent. Sci. 2018, 4, 1352−1359

http://pubs.acs.org/journal/acscii

PbS Capped $CsPbI_3$ Nanocrystals for Efficient and Stable Light-Emitting Devices Using *p*−*i*−*n* Structures

Xiaoyu Zhang,[†,‡,⊥] Min Lu,[†,⊥] Yu Zhang,[*,†] Hua Wu,[†] Xinyu Shen,[†] Wei Zhang,[‡] Weitao Zheng,[‡] Vicki L. Colvin,[§] and William W. Yu[†,∥]

[†]State Key Laboratory of Integrated Optoelectronics and College of Electronic Science and Engineering, Jilin University, Changchun 130012, China

[‡]Key Laboratory of Mobile Materials MOE, State Key Laboratory of Automotive Simulation and Control, and College of Materials Science, Jilin University, Changchun 130012, China

[§]Department of Chemistry, Brown University, Providence, Rhode Island 02912, United States

[∥]Department of Chemistry and Physics, Louisiana State University, Shreveport, Louisiana 71115, United States

Supporting Information

ABSTRACT: Cesium lead halide perovskite nanocrystals (NCs) have unique optical properties such as high color purity and high photoluminescence (PL) efficiency. However, the external quantum efficiency (EQE) of the corresponding light-emitting diodes (LEDs) is low, primarily as a result of the NC surface defects. Here, we report a method to reduce the surface defects by capping $CsPbI_3$ NCs with PbS. This passivation significantly enhanced the PL efficiency, reduced the Stokes shift, narrowed the PL bandwidth, and increased the stability of $CsPbI_3$ NCs. At the same time, $CsPbI_3$ NC films switched from *n*-type behavior to nearly ambipolar by PbS capping, which allowed us to fabricate electroluminescence LEDs using *p*−*i*−*n* structures. The thus-fabricated LEDs exhibited dramatically improved storage and operation stability, and an EQE of 11.8%. These results suggest that, with a suitable surface passivation strategy, the perovskite NCs are promising for next-generation LED and display applications.

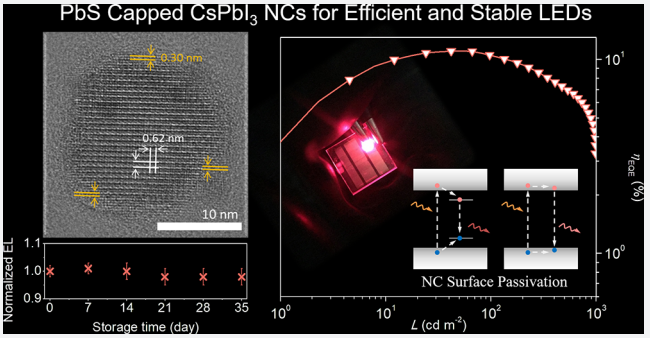

Lead halide perovskite nanocrystals (NCs) are promising for next-generation light-emitting diodes (LEDs) because of their high photoluminescence quantum yield (PL QY), narrow emission bandwidth, and wide color gamut.[1−5] The LED's external quantum efficiency (EQE) has risen quickly from <1% to over 10% thanks to the surface ligand density control, interface engineering, and other treatments.[6−23] The triple-ligand surface engineering strategy boosted the $CsPbBr_3$ NC ink's stability and the LED's EQE to 11.6%,[24] which takes advantage of the ionic nature of perovskite NCs as it is easy for them to lose their surface ligands,[25,26] revealing the important role of the NC surface.

On the other hand, the poor device stability still greatly impedes their practical applications. The rapid decomposition of perovskites in air limits the device storage and working lifetimes; their ion migration along crystal boundaries under bias can induce degradation and defects for nonradiative recombination, and thus harms the device operational stability.[27,28] Nowadays, several groups have improved the perovskite NC's stability using polyhedral oligomeric silsesquioxane, silica, and polymers[29−33] but at the expense of their semiconducting property, making them not suitable for active optoelectronic devices. Thus, it is urgent to find a way to stabilize the crystal surface and prevent ion migration without damaging the semiconductor property of perovskite NC films.

Epitaxial solution growth has shown great potential in colloidal chemistry to obtain core/shell structures to passivate the unsaturated core surface sites,[34] to reduce nonrecombination of photoexcited carriers,[35] to optimize the semiconductor property,[36] or to improve the material environmental stability.[37] However, to the best of our knowledge, there is no example showing successful epitaxial growth of one semiconductor on the surface of perovskite NCs. Typically, the lattice mismatch between two different materials should be less than 15% for successful epitaxial growth.[38] Sargent and coworkers demonstrated that perovskites and PbS can exhibit coherence in their lattice fringes due to their minimal lattice mismatch (<5%),[39−41] pointing out a great possibility in obtaining high-quality perovskite/PbS nanostructures.

Studies have shown that the synthesis of lead halide perovskite NCs occurs at room temperature because of their ion nature,[29] and the growth of perovskite on PbS is also feasible at room temperature.[40,42] In comparison, the synthesis

Received: June 21, 2018
Published: September 26, 2018

© 2018 American Chemical Society

DOI: 10.1021/acscentsci.8b00386
ACS Cent. Sci. 2018, 4, 1352−1359

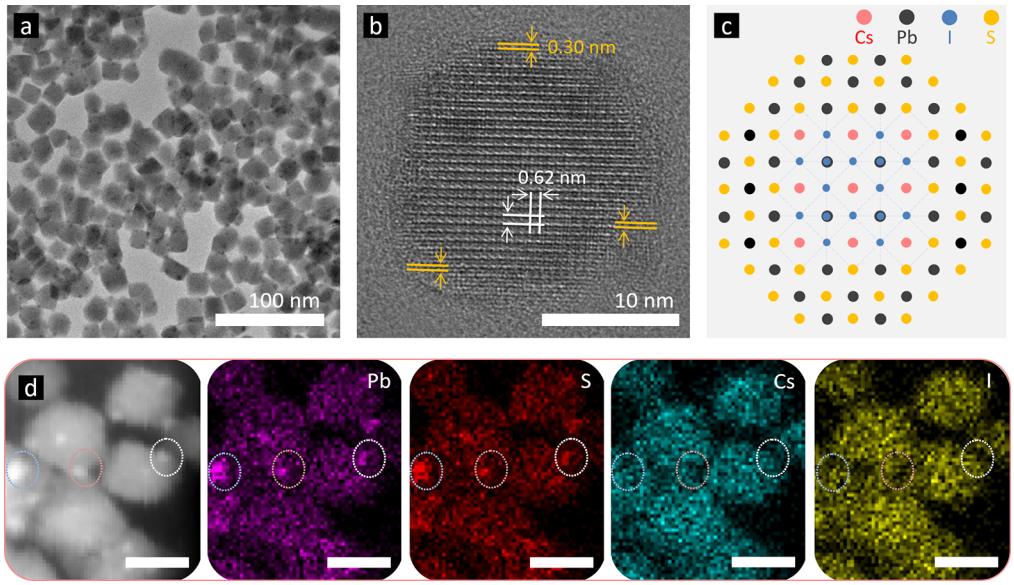

Figure 1. (a) TEM and (b) HRTEM images of $CsPbI_3$-0.1 NCs. (c) Proposed architecture of PbS capped $CsPbI_3$ NCs. (d) Elemental mapping of $CsPbI_3$-0.1 NCs. All scale bars represent 20 nm.

of covalent PbS NCs however needs high temperatures. We hypothesize that it may be possible to obtain PbS capped $CsPbI_3$ NCs when $CsPbI_3$ NCs are grown in a solution with ultrasmall PbS clusters available, through attaching these PbS clusters to the $CsPbI_3$ NC surfaces. This idea was realized in this study.

Here, we report a strategy to simultaneously enhance the optical properties and stability of perovskite NCs without damaging their semiconducting properties by capping the $CsPbI_3$ NCs with PbS. The surface defects of $CsPbI_3$ NCs were well passivated with PbS capping, which significantly enhanced the PL efficiency, reduced the Stokes shift, narrowed the PL spectrum, and increased the stability. The introduction of PbS capping made the NC films switch from *n*-type behavior to nearly ambipolar which allowed us to fabricate electroluminescence (EL) LEDs using *p*−*i*−*n* structures, which is known for efficient tunnel injection and flat band conditions under operation.[43] These *p*−*i*−*n* LEDs exhibited a low turn-on voltage of 1.9 V and an EQE of 10% at 2.3 V, and their peak EQE reached 11.8% at 2.8 V. Furthermore, the storage and operation stability of the unencapsulated devices in N_2 was also dramatically improved.

The $CsPbI_3$ NCs were synthesized following a modified procedure of Loredana et al.[1] The PbS capped $CsPbI_3$ NCs were prepared via injecting cesium oleate solution into a mixture of Pb^{2+}, I^-, and PbS clusters. The key point here is to control the growth of PbS clusters, which was realized by using a proper S precursor, thioacetamide, and optimizing the growth time. Thioacetamide has relatively low reactivity, allowing us to preciously optimize the size of PbS clusters. PbS capped $CsPbI_3$ perovskite NCs were synthesized with six S:Pb ratios of 0, 0.05, 0.075, 0.1, 0.15, and 0.2. The S:Pb ratios were determined from the molar ratios of the precursors (thioacetamide:PbI_2).

Transmission electron microscopy (TEM) was performed to characterize the structure of the as-prepared $CsPbI_3$-0.1 (meaning the molar ratio of S:Pb = 0.1) NCs. Their shape is between cubes and spheres (Figure 1a), which is different from the typical $CsPbI_3$ NC's regular cubic morphology. TEM images of other samples with different S:Pb ratios are given in Figure S1, showing that the number of cubic NCs decreases while spherical NCs increase when increasing the S content. At some points, $CsPbI_3$ NCs are found to connect with each other. Capping ligands are mostly coordinating at Pb sites for perovskite NCs,[44] and oleic acid can be removed through the formation of a Pb−S bond;[45] thus, when a PbS cluster is shared by two adjacent $CsPbI_3$ NCs, these two $CsPbI_3$ NCs will connect via PbS. This connection will improve the charge transport within the NC film and lead to better device performance.[39] The high-resolution TEM (HRTEM) image (Figure 1b) clearly shows two distinctive areas in one particle: a cubic core and a nonuniform shell around it. In the core, an interplanar distance of 0.62 nm was found, which is consistent with the (100) plane of cubic $CsPbI_3$.[46] In the shell, an interplanar distance of 0.30 nm was found, and this matches well with the (200) plane of PbS.[47] The $CsPbI_3$ NC core and PbS cap structure (Figure 2c) explain the roundish morphology of $CsPbI_3$-0.1. Additional HRTEM images are given in Figure S1, showing some thin PbS layer capped NCs from the $CsPbI_3$-0.05 sample (confirmed from the twisted lattice fringes, Figure S1e), and some thick PbS layer capped NCs from the $CsPbI_3$-0.2 sample (confirmed from the straight PbS lattice fringes, Figure S1f).

The elemental mapping (Figure 1d) shows the distribution of Cs, Pb, I, and S elements over the $CsPbI_3$-0.1 NCs. Some dots in light color, as circled, were found with enhanced concentrations in Pb and S element mapping images, and thus can be confirmed as PbS clusters. The HRTEM image showing a spherical dot attached on a $CsPbI_3$ NC in Figure S2 further identified this. Note that S and Pb elements were both uniformly distributed here, which is different from traditional CdSe/CdS core/shell quantum dots. As we discussed earlier, the formation of the PbS/perovskite interface is feasible at room temperature,[40] which will lead to S following the distribution of surface Pb elements. This was proven after we checked more HRTEM images of the PbS capped $CsPbI_3$ NCs shown in Figure S3; whether the $CsPbI_3$ NCs were capped by thin or thick shells, PbS was always found to take positions on

DOI: 10.1021/acscentsci.8b00386
ACS Cent. Sci. 2018, 4, 1352−1359

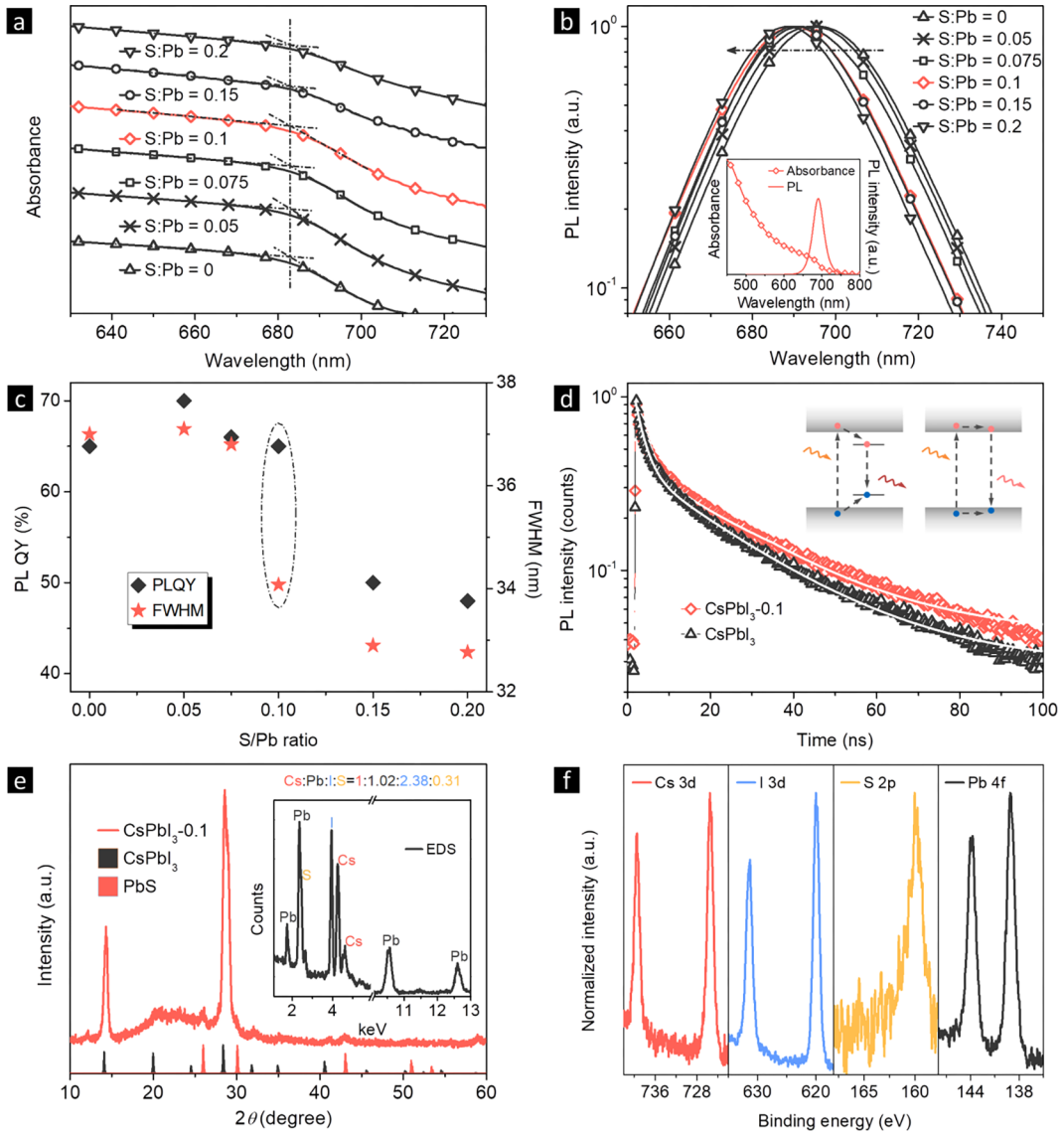

Figure 2. (a) Absorption and (b) PL spectra of $CsPbI_3$ NCs with different S:Pb ratios in toluene. Inset of part b shows the complete absorption and PL spectra of $CsPbI_3$-0.1 NCs. (c) PL QY and fwhm values as functions of S:Pb ratios. (d) TRPL curves of $CsPbI_3$ and $CsPbI_3$-0.1 NCs. (e) XRD pattern of $CsPbI_3$-0.1 NC film on quartz substrate, together with the reference patterns for bulk $CsPbI_3$ (black) and PbS (red). Inset is the EDS spectrum of the $CsPbI_3$-0.1 NCs. (f) XPS spectra of $CsPbI_3$-0.1 NCs.

the top of $CsPbI_3$ NCs. There would also be PbS attached on other sides of $CsPbI_3$ NCs with nonuniform thickness, leading to no particularly enhanced or decreased concentrations that follow the outline of the NC's shell in the element mapping images. The X-ray photoelectron spectroscopy (XPS) measurements of PbS capped $CsPbI_3$ NC film at a different depth (Figure S4) further demonstrate the difference between the composition of the core and the composition of the shell: a ~65% decrease in the S content was observed after removing a top layer by etching. There is no peak shift or shape change in the S 2p XPS spectra before and after etching, indicating the same chemical environment around S atoms. Thus, we conclude that S exists on the $CsPbI_3$ NC surface.

Now we have demonstrated that there is PbS in the final products from element mapping, and have proven that PbS is located on the $CsPbI_3$ NC surface. Since epitaxial growth is known to modify the NC surface and passivate defects, we used a series of optical property characterization to further confirm the successful capping of $CsPbI_3$ NCs with PbS. The transitions of absorption spectra (Figure 2a) for PbS capped $CsPbI_3$ perovskite NCs with different S:Pb ratios all located at 683 nm. In contrast, the PL peaks (Figure 2b) blue-shifted from 695 to 688 nm as the S:Pb ratio increased from 0 to 0.2. At the same time, the PL peak's full-width at half-maximum (fwhm) decreased from 37 to 33 nm. The absorption and PL spectra of $CsPbI_3$-0.1 NCs are given as the inset of Figure 2b, showing the typical spectra of conventional perovskite NCs. Photos of $CsPbI_3$-0.1 NC toluene solution under daylight and 365 nm excited are given in Figure S5, revealing that the NC solution is perfectly transparent. The tail states in the absorption spectrum may originate from the small PbS particles.

The absolute PL QY and fwhm as functions of the S:Pb ratios are summarized in Figure 2c. The PL QY increased from 65% to 70% when the S:Pb ratio varied from 0 to 0.05, and then decreased to 66%, 65%, 50%, and 48% when the S:Pb ratio increased to 0.075, 0.1, 0.15, and 0.2, respectively. The $CsPbI_3$-0.1 NCs showed both high PL QY (65%) and superior

DOI: 10.1021/acscentsci.8b00386
ACS Cent. Sci. 2018, 4, 1352−1359

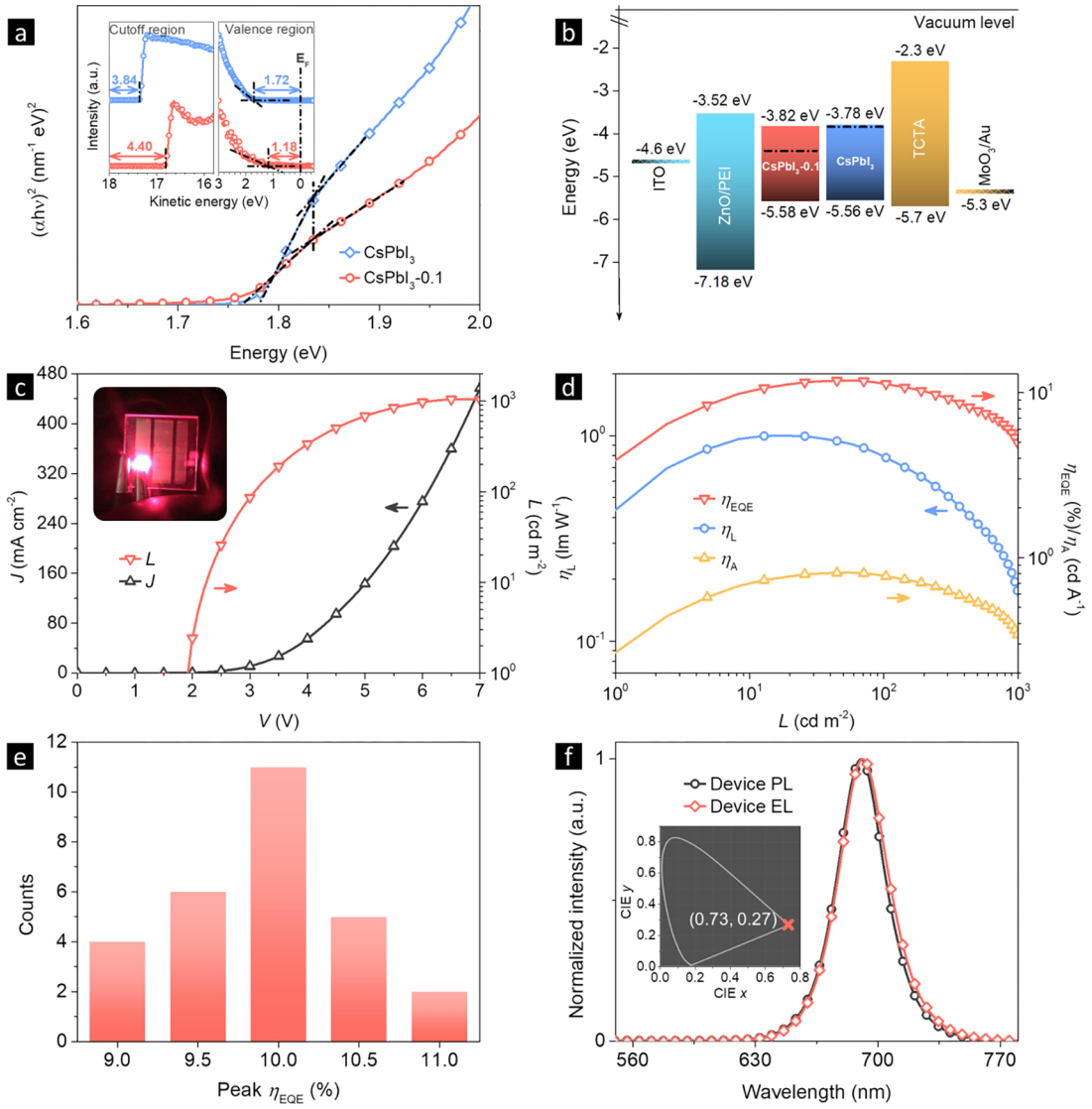

Figure 3. (a) Tauc plots of $CsPbI_3$ and $CsPbI_3$-0.1 NC films with their UPS spectra. (b) Device energy level diagram for all functional layers. (c) *J*–*V*–*L* curves with a working device photo. (d) EQE, η_A, and η_L versus brightness. (e) Peak EQEs collected from 28 devices. (f) PL and EL spectra of the $CsPbI_3$-0.1 NC LED; inset shows the corresponding CIE coordinates for the EL spectrum.

color purity (fwhm of 34 nm); thus, they were chosen for further research.

Time-resolved PL (TRPL) spectroscopy was carried out on pure and $CsPbI_3$-0.1 NCs. It can be seen from Figure 2d that the PL average lifetime increases from 16.9 to 17.4 ns with the S:Pb ratio change from 0 to 0.1 (Table S1). As shown in the Figure 2d inset, the spontaneous radiative recombination between trap states generally leads to a lower energy emission compared with that from the band edge transition, and passivation of these trap states can blue-shift the PL peak.[48] Additionally, the PL peak was narrowed, and the PL QY was increased by introducing PbS. We thus conclude that the NC's surface defects have been successfully passivated.

Figure 2e presents the X-ray diffraction (XRD) pattern of the $CsPbI_3$-0.1 NC film. The diffraction peaks of both cubic $CsPbI_3$ and PbS can be seen which indicates the existence of two individual phases. The chemical composition of the $CsPbI_3$-0.1 NCs was analyzed via energy dispersive spectroscopy (EDS). As given in the Figure 2e inset, elements of Cs, Pb, I, and S are identified, and the elemental ratio of Cs:Pb:I:S is found to be 1:1.02:2.38:0.31. All elements were further confirmed with XPS (Figure 2f), and the results are consistent with EDS. No new peak appears in the FTIR spectra after PbS capping (Figure S6), indicating that $CsPbI_3$ and $CsPbI_3$-0.1 NCs have the same surface ligands, and thioacetamide does not serve as ligands here.

The Tauc plots and ultraviolet photoelectron spectroscopy (UPS) spectra of $CsPbI_3$ and $CsPbI_3$-0.1 NCs are given in Figure 3a. For pure $CsPbI_3$ NCs, their Fermi level (−3.84 eV) and CBM (conduction band minimum, −3.78 eV) are close, clearly identifying their *n*-type behavior (Figure 3b). After PbS capping, the Fermi level shifts to −4.40 eV while the CBM and VBM (valence band maximum) values are unchanged, demonstrating the switch from *n*-type to nearly ambipolar (Figure S7). The surface chemistry of $CsPbI_3$ NCs is different after PbS capping and thus changes the electronic property.[49]

The nearly ambipolar behavior of $CsPbI_3$-0.1 NCs allowed us to build LEDs using *p*–*i*–*n* structures. The device energy band diagram for all functional layers is given in Figure 3b. A wide bandgap *n*-type ZnO NC film was chosen as both the

DOI: 10.1021/acscentsci.8b00386
ACS Cent. Sci. 2018, 4, 1352−1359

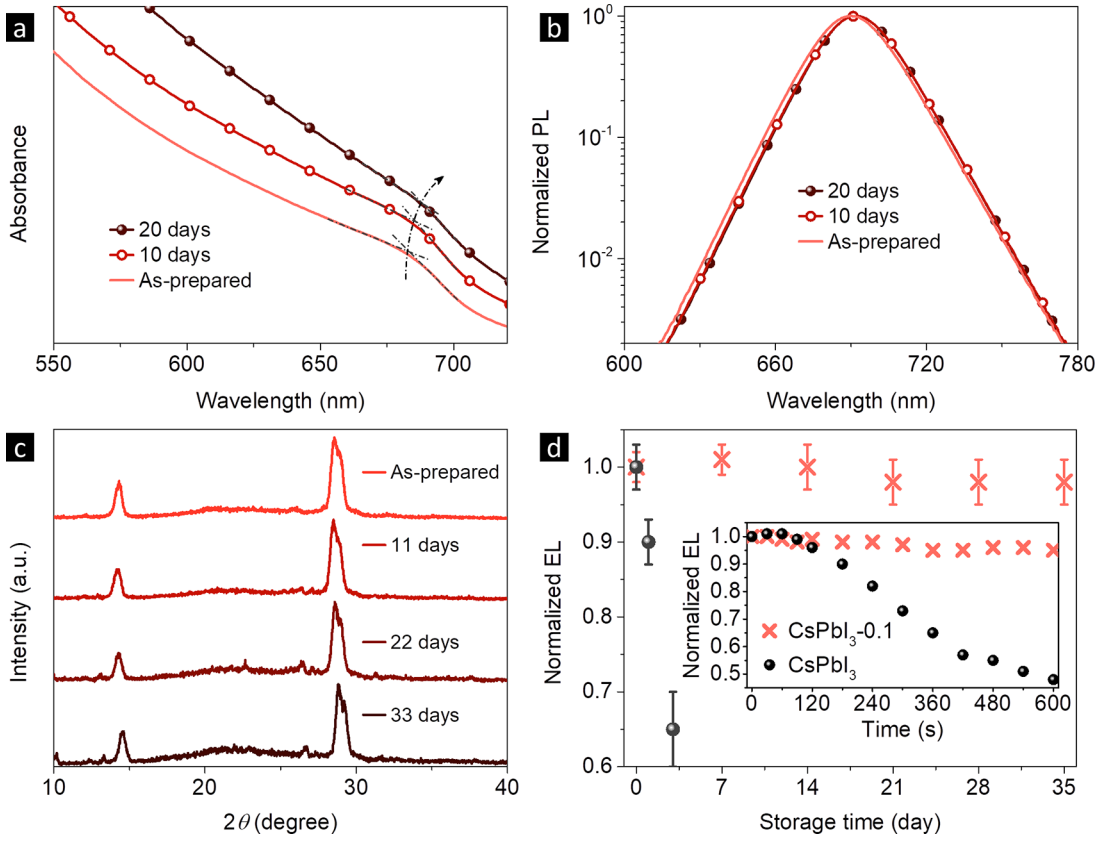

Figure 4. (a) Absorption and (b) PL spectra of $CsPbI_3$-0.1 NC toluene solution stored in air for 20 days. (c) Film XRD patterns of $CsPbI_3$-0.1 NCs stored in ambient conditions for 33 days. (d) Time-related storage stability of $CsPbI_3$ and $CsPbI_3$-0.1 NC LEDs in nitrogen. Inset shows time-related EL intensities of pure and $CsPbI_3$-0.1 NC devices at the same voltage of 2.5 V.

electron transport layer (ETL) and the hole blocking layer (HBL) because of its excellent optical transparency and deep lying VBM.[50] A *p*-type 4,4′,4″-tris(carbazol-9-yl)-triphenylamine (TCTA) film was chosen as the hole transport layer (HTL) and also the electron blocking layer (EBL) because of its suitable HOMO (highest occupied molecular orbital) and low electron affinity. The combination of ZnO and TCTA allows effective confinement of injected charge carriers in the emissive layer for radiative recombination. MoO_3/Au and ITO/ZnO/polyethylenimine were used as the top and bottom electrodes, respectively, for their ohmic carrier injection property.[51,52]

Figure 3c presents the *J*−*V*−*L* curves of the $CsPbI_3$-0.1 NC LEDs and a working device with a 9 mm^2 emitting area. The devices had a low turn-on voltage of 1.9 V, which is close to the band gap energy of the emitters (1.78 eV), meaning that a highly efficient and barrier-free charge injection into the NC emitters was achieved.[53] The luminance reached 1050 cd m^{-2} maximum at 6.7 V voltage and 397 mA cm^{-2} current density. A peak EQE of 11.8% was achieved at 2.8 V (Figure 3d). The low-efficiency roll-off (7.6% of the EQE was preserved at 100 mA cm^{-2}) indicates that the NCs kept a low charging degree even at high current densities.[54] The peak current efficiency (η_A) and power efficiency (η_L) of the device were 0.81 cd A^{-1} and 0.99 lm W^{-1}, respectively. Figure 3e shows an average peak EQE of 10% from 28 devices. $CsPbI_3$ NC LEDs with the same parameters were fabricated and compared (Figure S8).

Figure 3f displays normalized PL and EL spectra of a typical $CsPbI_3$-0.1 NC LED (Figure S9). Apparently the EL was from $CsPbI_3$ NCs without noticeable contribution from any charge transport materials. Therefore, the NCs were the exciton recombination centers for the device, and a balanced charge carrier transport was achieved.[55,56] The symmetric emission corresponds to Commission Internationale de l'Eclairage (CIE) color coordinates of (0.73, 0.27).

The transformation from cubic to orthorhombic phase of $CsPbI_3$ NCs deteriorates their appealing semiconducting properties[46,57] and greatly hinders their practical applications. Pure $CsPbI_3$ NCs showed poor solution stability, and turned from deep red to yellow in 3 days in air, similar to the published results.[46,58] In comparison, both absorption and PL spectra of $CsPbI_3$-0.1 NC solution only experienced a slight red-shift after 20 days, while the solution color remained the same (deep red) (Figure 4a,b), representing a much better solution stability.

The phase stability of NC films is crucial for LED and solar cell applications. As shown in Figure 4c, XRD patterns of $CsPbI_3$-0.1 NC films demonstrate that the NCs remained in cubic phase even after 33 days of storage in ambient conditions, demonstrating the greatly enhanced phase stability by PbS capping. The storage stability of unencapsulated NC LEDs stored in nitrogen was also evaluated. Figure 4d shows that the EL intensity of $CsPbI_3$-0.1 LEDs is very stable with ignorable change after being stored for 35 days, while the EL intensity of pure $CsPbI_3$ LEDs decreased by 30−40% in 3 days. The significantly improved stability of the $CsPbI_3$-0.1 LEDs can be attributed to the PbS shell that stabilizes the crystallite surface.[59,60] Stable $CsPbI_3$-0.1 NC films also empower improved device operation stability (Figure 4d inset, Figure S10). To avoid the impact from Joule heating, the devices were

DOI: 10.1021/acscentsci.8b00386
ACS Cent. Sci. 2018, 4, 1352−1359

operated at a low voltage of 2.5 V. The EL intensity of pure $CsPbI_3$ LEDs dropped to 48% of their initial value in 600 s, while the EL intensity of $CsPbI_3$-0.1 LEDs showed a negligible change. Ion migration in perovskite films has been proven to induce degradation and generate nonradiative recombination sites in the emissive layer, which is responsible for the operation instability.[28] We thus conclude that PbS capping can help to stabilize the NC surface and impede ion migration of NC films (Figure S11). Improving charge injection through interface engineering to operate LEDs at lower voltages would further enhance the operation stability of the PbS capped $CsPbI_3$ NC devices.

In conclusion, we have shown that PbS capping can dramatically passivate the surface defects and enhance the optical and phase stability of $CsPbI_3$ NCs. Surface defect passivation induces enhanced PL efficiency, reduced Stokes shift, and narrowed PL spectrum. PbS capping also helps stabilize the NC surface and impede ion migration, thus significantly improving the device storage and operation stability. At the same time, $CsPbI_3$ NC films switched from *n*-type behavior to nearly ambipolar by PbS capping, which allowed us to make EL LEDs with *p*−*i*−*n* structures. As a result, the LEDs made from $CsPbI_3$-0.1 showed greatly improved performance including an EQE of 11.8%, and an average peak EQE of 10%. It is also worth investigating whether the PbS capping of perovskite NCs can benefit other devices such as solar cells, photodetectors, and lasers.

■ ASSOCIATED CONTENT

Supporting Information

The Supporting Information is available free of charge on the ACS Publications website at DOI: 10.1021/acscentsci.8b00386.

Additional synthesis and characterization details, TEM and HRTEM images, XPS and FTIR spectra, semiconductor property analysis, angle dependent EL spectra, device operational stability, and hysteresis loop analysis (PDF)

■ AUTHOR INFORMATION

Corresponding Author

*E-mail: yuzhang@jlu.edu.cn.

ORCID

Yu Zhang: 0000-0003-2100-621X

Wei Zhang: 0000-0002-6414-7015

William W. Yu: 0000-0001-5354-6718

Author Contributions

⊥X.Z. and M.L. contributed equally.

Notes

The authors declare no competing financial interest.

No unexpected or unusually high safety hazards were encountered.

■ ACKNOWLEDGMENTS

The authors thank the Natural Science Foundation of China (61675086, 61475062, 61722504, 51702115, 51772123), National Key Research and Development Program of China (2017YFB0403601), China Postdoctoral Science Foundation (2017M611319), National Postdoctoral Program for Innovative Talents (BX201600060), BORSF RCS, Institutional Development Award (P20GM103424), and Open Research Fund of State Key Laboratory of Polymer Physics and Chemistry, Changchun Institute of Applied Chemistry, Chinese Academy of Sciences.

■ REFERENCES

(1) Protesescu, L.; Yakunin, S.; Bodnarchuk, M. I.; Krieg, F.; Caputo, R.; Hendon, C. H.; Yang, R. X.; Walsh, A.; Kovalenko, M. V. Nanocrystals of Cesium Lead Halide Perovskites ($CsPbX_3$, X = Cl, Br, and I): Novel Optoelectronic Materials Showing Bright Emission with Wide Color Gamut. *Nano Lett.* **2015**, *15*, 3692−3696.

(2) Zhang, F.; Zhong, H.; Chen, C.; Wu, X.-g.; Hu, X.; Huang, H.; Han, J.; Zou, B.; Dong, Y. Brightly Luminescent and Color-Tunable Colloidal $CH_3NH_3PbX_3$ (X = Br, I, Cl) Quantum Dots: Potential Alternatives for Display Technology. *ACS Nano* **2015**, *9*, 4533−4542.

(3) Hu, F.; Zhang, H.; Sun, C.; Yin, C.; Lv, B.; Zhang, C.; Yu, W. W.; Wang, X.; Zhang, Y.; Xiao, M. Superior Optical Properties of Perovskite Nanocrystals as Single Photon Emitters. *ACS Nano* **2015**, *9*, 12410−12416.

(4) Xu, Y.; Chen, Q.; Zhang, C.; Wang, R.; Wu, H.; Zhang, X.; Xing, G.; Yu, W. W.; Wang, X.; Zhang, Y.; Xiao, M. Two-Photon-Pumped Perovskite Semiconductor Nanocrystal Lasers. *J. Am. Chem. Soc.* **2016**, *138*, 3761−3768.

(5) Yan, F.; Xing, J.; Xing, G.; Quan, L.; Tan, S. T.; Zhao, J.; Su, R.; Zhang, L.; Chen, S.; Zhao, Y.; Huan, A.; Sargent, E. H.; Xiong, Q.; Demir, H. V. Highly Efficient Visible Colloidal Lead-Halide Perovskite Nanocrystal Light-Emitting Diodes. *Nano Lett.* **2018**, *18*, 3157−3164.

(6) Song, J.; Li, J.; Li, X.; Xu, L.; Dong, Y.; Zeng, H. Quantum Dot Light-Emitting Diodes Based on Inorganic Perovskite Cesium Lead Halides ($CsPbX_3$). *Adv. Mater.* **2015**, *27*, 7162−7167.

(7) Zhang, X.; Lin, H.; Huang, H.; Reckmeier, C.; Zhang, Y.; Choy, W. C. H.; Rogach, A. L. Enhancing the Brightness of Cesium Lead Halide Perovskite Nanocrystal Based Green Light-Emitting Devices through the Interface Engineering with Perfluorinated Ionomer. *Nano Lett.* **2016**, *16*, 1415−1420.

(8) Zhang, X.; Sun, C.; Zhang, Y.; Wu, H.; Ji, C.; Chuai, Y.; Wang, P.; Wen, S.; Zhang, C.; Yu, W. W. Bright Perovskite Nanocrystal Films for Efficient Light-Emitting Devices. *J. Phys. Chem. Lett.* **2016**, *7*, 4602−4610.

(9) Zhang, X.; Xu, B.; Zhang, J.; Gao, Y.; Zheng, Y.; Wang, K.; Sun, X. W. All-Inorganic Perovskite Nanocrystals for High-Efficiency Light Emitting Diodes: Dual-Phase $CsPbBr_3$-$CsPb_2Br_5$ Composites. *Adv. Funct. Mater.* **2016**, *26*, 4595−4600.

(10) Li, J.; Xu, L.; Wang, T.; Song, J.; Chen, J.; Xue, J.; Dong, Y.; Cai, B.; Shan, Q.; Han, B.; Zeng, H. 50-Fold EQE Improvement up to 6.27% of Solution-Processed All-Inorganic Perovskite $CsPbBr_3$ QLEDs via Surface Ligand Density Control. *Adv. Mater.* **2017**, *29*, 1603885.

(11) Chiba, T.; Hoshi, K.; Pu, Y.-J.; Takeda, Y.; Hayashi, Y.; Ohisa, S.; Kawata, S.; Kido, J. High-Efficiency Perovskite Quantum-Dot Light-Emitting Devices by Effective Washing Process and Interfacial Energy Level Alignment. *ACS Appl. Mater. Interfaces* **2017**, *9*, 18054−18060.

(12) Huang, H.; Zhao, F.; Liu, L.; Zhang, F.; Wu, X.-g.; Shi, L.; Zou, B.; Pei, Q.; Zhong, H. Emulsion Synthesis of Size-Tunable $CH_3NH_3PbBr_3$ Quantum Dots: An Alternative Route toward Efficient Light-Emitting Diodes. *ACS Appl. Mater. Interfaces* **2015**, *7*, 28128−28133.

(13) Kumar, S.; Jagielski, J.; Kallikounis, N.; Kim, Y.-H.; Wolf, C.; Jenny, F.; Tian, T.; Hofer, C. J.; Chiu, Y.-C.; Stark, W. J.; Lee, T.-W.; Shih, C.-J. Ultrapure Green Light-Emitting Diodes Using Two-Dimensional Formamidinium Perovskites: Achieving Recommendation 2020 Color Coordinates. *Nano Lett.* **2017**, *17*, 5277−5284.

(14) Yao, E.-P.; Yang, Z.; Meng, L.; Sun, P.; Dong, S.; Yang, Y.; Yang, Y. High-Brightness Blue and White LEDs based on Inorganic Perovskite Nanocrystals and their Composites. *Adv. Mater.* **2017**, *29*, 1606859.

(15) Zhao, L.; Yeh, Y.-W.; Tran, N. L.; Wu, F.; Xiao, Z.; Kerner, R. A.; Lin, Y. L.; Scholes, G. D.; Yao, N.; Rand, B. P. In Situ Preparation of Metal Halide Perovskite Nanocrystal Thin Films for Improved Light-Emitting Devices. *ACS Nano* **2017**, *11*, 3957−3964.
(16) Kumar, S.; Jagielski, J.; Yakunin, S.; Rice, P.; Chiu, Y.-C.; Wang, M.; Nedelcu, G.; Kim, Y.; Lin, S.; Santos, E. J. G.; Kovalenko, M. V.; Shih, C.-J. Efficient Blue Electroluminescence Using Quantum-Confined Two-Dimensional Perovskites. *ACS Nano* **2016**, *10*, 9720−9729.
(17) Wu, H.; Zhang, Y.; Zhang, X.; Lu, M.; Sun, C.; Zhang, T.; Yu, W. W. Enhanced Stability and Performance in Perovskite Nanocrystal Light-Emitting Devices Using a ZnMgO Interfacial Layer. *Adv. Opt. Mater.* **2017**, *5*, 1700377.
(18) Pan, G.; Bai, X.; Yang, D.; Chen, X.; Jing, P.; Qu, S.; Zhang, L.; Zhou, D.; Zhu, J.; Xu, W.; Dong, B.; Song, H. Doping Lanthanide into Perovskite Nanocrystals: Highly Improved and Expanded Optical Properties. *Nano Lett.* **2017**, *17*, 8005−8011.
(19) Zeng, Q.; Zhang, X.; Feng, X.; Lu, S.; Chen, Z.; Yong, X.; Redfern, S. A. T.; Wei, H.; Wang, H.; Shen, H.; Zhang, W.; Zheng, W.; Zhang, H.; Tse, J. S.; Yang, B. Polymer-Passivated Inorganic Cesium Lead Mixed-Halide Perovskites for Stable and Efficient Solar Cells with High Open-Circuit Voltage over 1.3 V. *Adv. Mater.* **2018**, *30*, 1705393.
(20) Zhang, X.; Bai, X.; Wu, H.; Zhang, X.; Sun, C.; Zhang, Y.; Zhang, W.; Zheng, W.; Yu, W. W.; Rogach, A. L. Water-Assisted Size and Shape Control of $CsPbBr_3$ Perovskite Nanocrystals. *Angew. Chem., Int. Ed.* **2018**, *57*, 3337−3342.
(21) Yao, J.; Ge, J.; Han, B.; Wang, K.; Yao, H.; Yu, H.; Li, J.; Zhu, B.; Song, J.; Chen, C.; Zhang, Q.; Zeng, H.; Luo, Y.; Yu, S. Ce^{3+}-Doping to Modulate Photoluminescence Kinetics for Efficient $CsPbBr_3$ Nanocrystals Based Light-Emitting Diodes. *J. Am. Chem. Soc.* **2018**, *140*, 3626−3634.
(22) Pan, J.; Shang, Y.; Yin, J.; De Bastiani, M.; Peng, W.; Dursun, I.; Sinatra, L.; El-Zohry, A. M.; Hedhili, M. N.; Emwas, A.-H.; Mohammed, O. F.; Ning, Z.; Bakr, O. M. Bidentate Ligand-Passivated $CsPbI_3$ Perovskite Nanocrystals for Stable Near-Unity Photoluminescence Quantum Yield and Efficient Red Light-Emitting Diodes. *J. Am. Chem. Soc.* **2018**, *140*, 562−565.
(23) Lu, M.; Zhang, X.; Bai, X.; Wu, H.; Shen, X.; Zhang, Y.; Zhang, W.; Zheng, W.; Song, H.; Yu, W. W.; Rogach, A. L. Spontaneous Silver Doping and Surface Passivation of $CsPbI_3$ Perovskite Active Layer Enable Light-Emitting Devices with an External Quantum Efficiency of 11.2%. *ACS Energy Lett.* **2018**, *3*, 1571−1577.
(24) Song, J.; Li, J.; Xu, L.; Li, J.; Zhang, F.; Han, B.; Shan, Q.; Zeng, H. Room-Temperature Triple-Ligand Surface Engineering Synergistically Boosts Ink Stability, Recombination Dynamics, and Charge Injection toward EQE-11.6% Perovskite QLEDs. *Adv. Mater.* **2018**, *30*, 1800764.
(25) Li, X.; Yu, D.; Cao, F.; Gu, Y.; Wei, Y.; Wu, Y.; Song, J.; Zeng, H. Healing All-Inorganic Perovskite Films via Recyclable Dissolution−Recyrstallization for Compact and Smooth Carrier Channels of Optoelectronic Devices with High Stability. *Adv. Funct. Mater.* **2016**, *26*, 5903−5912.
(26) Kim, Y.; Yassitepe, E.; Voznyy, O.; Comin, R.; Walters, G.; Gong, X.; Kanjanaboos, P.; Nogueira, A. F.; Sargent, E. H. Efficient Luminescence from Perovskite Quantum Dot Solids. *ACS Appl. Mater. Interfaces* **2015**, *7*, 25007−25013.
(27) De Roo, J.; Ibáñez, M.; Geiregat, P.; Nedelcu, G.; Walravens, W.; Maes, J.; Martins, J. C.; Van Driessche, I.; Kovalenko, M. V.; Hens, Z. Highly Dynamic Ligand Binding and Light Absorption Coefficient of Cesium Lead Bromide Perovskite Nanocrystals. *ACS Nano* **2016**, *10*, 2071−2081.
(28) Xiao, Z.; Kerner, R. A.; Zhao, L.; Tran, N. L.; Lee, K. M.; Koh, T.-W.; Scholes, G. D.; Rand, B. P. Efficient Perovskite Light-Emitting Diodes Featuring Nanometre-Sized Crystallites. *Nat. Photonics* **2017**, *11*, 108−115.
(29) Li, X.; Wu, Y.; Zhang, S.; Cai, B.; Gu, Y.; Song, J.; Zeng, H. $CsPbX_3$ Quantum Dots for Lighting and Displays: Room-Temperature Synthesis, Photoluminescence Superiorities, Underlying Origins and White Light-Emitting Diodes. *Adv. Funct. Mater.* **2016**, *26*, 2435−2445.
(30) Liu, P.; Chen, W.; Wang, W.; Xu, B.; Wu, D.; Hao, J.; Cao, W.; Fang, F.; Li, Y.; Zeng, Y.; Pan, R.; Chen, S.; Cao, W.; Sun, X. W.; Wang, K. Halide-Rich Synthesized Cesium Lead Bromide Perovskite Nanocrystals for Light-Emitting Diodes with Improved Performance. *Chem. Mater.* **2017**, *29*, 5168−5173.
(31) Huang, H.; Chen, B.; Wang, Z.; Hung, T. F.; Susha, A. S.; Zhong, H.; Rogach, A. L. Water Resistant $CsPbX_3$ Nanocrystals Coated with Polyhedral Oligomeric Silsesquioxane and Their Use as Solid State Luminophores in All-Perovskite White Light-Emitting Devices. *Chem. Sci.* **2016**, *7*, 5699−5703.
(32) Sun, C.; Zhang, Y.; Ruan, C.; Yin, C.; Wang, X.; Wang, Y.; Yu, W. W. Efficient and Stable White LEDs with Silica-Coated Inorganic Perovskite Quantum Dots. *Adv. Mater.* **2016**, *28*, 10088−10094.
(33) Wang, Y.; He, J.; Chen, H.; Chen, J.; Zhu, R.; Ma, P.; Towers, A.; Lin, Y.; Gesquiere, A. J.; Wu, S.-T.; Dong, Y. Ultrastable, Highly Luminescent Organic−Inorganic Perovskite−Polymer Composite Films. *Adv. Mater.* **2016**, *28*, 10710−10717.
(34) Mews, A.; Kadavanich, A. V.; Banin, U.; Alivisatos, A. P. Structural and Spectroscopic Investigations of CdS/HgS/CdS Quantum-Dot Quantum Wells. *Phys. Rev. B: Condens. Matter Mater. Phys.* **1996**, *53*, R13242−R13245.
(35) Peng, X.; Schlamp, M. C.; Kadavanich, A. V.; Alivisatos, A. P. Epitaxial Growth of Highly Luminescent CdSe/CdS Core/Shell Nanocrystals with Photostability and Electronic Accessibility. *J. Am. Chem. Soc.* **1997**, *119*, 7019−7029.
(36) Yang, Z.; Janmohamed, A.; Lan, X.; García de Arquer, F. P.; Voznyy, O.; Yassitepe, E.; Kim, G.-H.; Ning, Z.; Gong, X.; Comin, R.; Sargent, E. H. Colloidal Quantum Dot Photovoltaics Enhanced by Perovskite Shelling. *Nano Lett.* **2015**, *15*, 7539−7543.
(37) Reiss, P.; Protiere, M.; Li, L. Core/Shell Semiconductor Nanocrystals. *Small* **2009**, *5*, 154−168.
(38) Tan, C.; Chen, J.; Wu, X.-J.; Zhang, H. Epitaxial Growth of Hybrid Nanostructures. *Nature Reviews Materials* **2018**, *3*, 17089.
(39) Gong, X.; Yang, Z.; Walters, G.; Comin, R.; Ning, Z.; Beauregard, E.; Adinolfi, V.; Voznyy, O.; Sargent, E. H. Highly Efficient Quantum Dot Near-Infrared Light-Emitting Diodes. *Nat. Photonics* **2016**, *10*, 253−257.
(40) Ning, Z.; Gong, X.; Comin, R.; Walters, G.; Fan, F.; Voznyy, O.; Yassitepe, E.; Buin, A.; Hoogland, S.; Sargent, E. H. Quantum-Dot-in-Perovskite Solids. *Nature* **2015**, *523*, 324.
(41) Xu, J.; Voznyy, O.; Liu, M.; Kirmani, A. R.; Walters, G.; Munir, R.; Abdelsamie, M.; Proppe, A. H.; Sarkar, A.; García de Arquer, F. P.; Wei, M.; Sun, B.; Liu, M.; Ouellette, O.; Quintero-Bermudez, R.; Li, J.; Fan, J.; Quan, L.; Todorovic, P.; Tan, H.; Hoogland, S.; Kelley, S. O.; Stefik, M.; Amassian, A.; Sargent, E. H. 2D Matrix Engineering for Homogeneous Quantum Dot Coupling in Photovoltaic Solids. *Nat. Nanotechnol.* **2018**, *13*, 456−462.
(42) Sytnyk, M.; Yakunin, S.; Schöfberger, W.; Lechner, R. T.; Burian, M.; Ludescher, L.; Killilea, N. A.; YousefiAmin, A.; Kriegner, D.; Stangl, J.; Groiss, H.; Heiss, W. Quasi-Epitaxial Metal-Halide Perovskite Ligand Shells on PbS Nanocrystals. *ACS Nano* **2017**, *11*, 1246−1256.
(43) Huang, J.; Pfeiffer, M.; Werner, A.; Blochwitz, J.; Leo, K.; Liu, S. Low-Voltage Organic Electroluminescent Devices Using PIN Structures. *Appl. Phys. Lett.* **2002**, *80*, 139−141.
(44) Huang, H.; Raith, J.; Kershaw, S. V.; Kalytchuk, S.; Tomanec, O.; Jing, L.; Susha, A. S.; Zboril, R.; Rogach, A. L. Growth Mechanism of Strongly Emitting $CH_3NH_3PbBr_3$ Perovskite Nanocrystals with A Tunable Bandgap. *Nat. Commun.* **2017**, *8*, 996.
(45) Tang, J.; Brzozowski, L.; Barkhouse, D. A. R.; Wang, X.; Debnath, R.; Wolowiec, R.; Palmiano, E.; Levina, L.; Pattantyus-Abraham, A. G.; Jamakosmanovic, D.; Sargent, E. H. Quantum Dot Photovoltaics in the Extreme Quantum Confinement Regime: The Surface-Chemical Origins of Exceptional Air- and Light-Stability. *ACS Nano* **2010**, *4*, 869−878.

DOI: 10.1021/acscentsci.8b00386
ACS Cent. Sci. 2018, 4, 1352−1359

(46) Wang, C.; Chesman, A. S. R.; Jasieniak, J. J. Stabilizing the Cubic Perovskite Phase of $CsPbI_3$ Nanocrystals by Using an Alkyl Phosphinic Acid. *Chem. Commun.* **2017**, *53*, 232−235.
(47) Zhao, H.; Chaker, M.; Wu, N.; Ma, D. Towards Controlled Synthesis and Better Understanding of Highly Luminescent PbS/CdS Core/Shell Quantum Dots. *J. Mater. Chem.* **2011**, *21*, 8898−8904.
(48) Shao, Y.; Xiao, Z.; Bi, C.; Yuan, Y.; Huang, J. Origin and Elimination of Photocurrent Hysteresis by Fullerene Passivation in $CH_3NH_3PbI_3$ Planar Heterojunction Solar Cells. *Nat. Commun.* **2014**, *5*, 5784.
(49) Brown, P. R.; Kim, D.; Lunt, R. R.; Zhao, N.; Bawendi, M. G.; Grossman, J. C.; Bulović, V. Energy Level Modification in Lead Sulfide Quantum Dot Thin Films through Ligand Exchange. *ACS Nano* **2014**, *8*, 5863−5872.
(50) Wang, J.; Wang, N.; Jin, Y.; Si, J.; Tan, Z.-K.; Du, H.; Cheng, L.; Dai, X.; Bai, S.; He, H.; Ye, Z.; Lai, M. L.; Friend, R. H.; Huang, W. Interfacial Control Toward Efficient and Low-Voltage Perovskite Light-Emitting Diodes. *Adv. Mater.* **2015**, *27*, 2311−2316.
(51) Li, C.; Credgington, D.; Ko, D.-H.; Rong, Z.; Wang, J.; Greenham, N. C. Built-in Potential Shift and Schottky-Barrier Narrowing in Organic Solar Cells with UV-Sensitive Electron Transport Layers. *Phys. Chem. Chem. Phys.* **2014**, *16*, 12131−12136.
(52) Zhou, Y.; Fuentes-Hernandez, C.; Shim, J.; Meyer, J.; Giordano, A. J.; Li, H.; Winget, P.; Papadopoulos, T.; Cheun, H.; Kim, J.; Fenoll, M.; Dindar, A.; Haske, W.; Najafabadi, E.; Khan, T. M.; Sojoudi, H.; Barlow, S.; Graham, S.; Brédas, J.-L.; Marder, S. R.; Kahn, A.; Kippelen, B. A Universal Method to Produce Low−Work Function Electrodes for Organic Electronics. *Science* **2012**, *336*, 327−332.
(53) Kwak, J.; Bae, W. K.; Lee, D.; Park, I.; Lim, J.; Park, M.; Cho, H.; Woo, H.; Yoon, D. Y.; Char, K. Bright and Efficient Full-Color Colloidal Quantum Dot Light-Emitting Diodes Using an Inverted Device Structure. *Nano Lett.* **2012**, *12*, 2362−2366.
(54) Dai, X.; Zhang, Z.; Jin, Y.; Niu, Y.; Cao, H.; Liang, X.; Chen, L.; Wang, J.; Peng, X. Solution-Processed, High-Performance Llight-Emitting Diodes Based on Quantum Dots. *Nature* **2014**, *515*, 96−99.
(55) Bae, W. K.; Park, Y.-S.; Lim, J.; Lee, D.; Padilha, L. A.; McDaniel, H.; Robel, I.; Lee, C.; Pietryga, J. M.; Klimov, V. I. Controlling the Influence of Auger Recombination on the Performance of Quantum-Dot Light-Emitting Diodes. *Nat. Commun.* **2013**, *4*, 2661.
(56) Brovelli, S.; Bae, W. K.; Galland, C.; Giovanella, U.; Meinardi, F.; Klimov, V. I. Dual-Color Electroluminescence from Dot-in-Bulk Nanocrystals. *Nano Lett.* **2014**, *14*, 486−494.
(57) Swarnkar, A.; Marshall, A. R.; Sanehira, E. M.; Chernomordik, B. D.; Moore, D. T.; Christians, J. A.; Chakrabarti, T.; Luther, J. M. Quantum Dot−Induced Phase Stabilization of α-$CsPbI_3$ Perovskite for High-Efficiency Photovoltaics. *Science* **2016**, *354*, 92−95.
(58) Zhang, F.; Huang, S.; Wang, P.; Chen, X.; Zhao, S.; Dong, Y.; Zhong, H. Colloidal Synthesis of Air-Stable $CH_3NH_3PbI_3$ Quantum Dots by Gaining Chemical Insight into the Solvent Effects. *Chem. Mater.* **2017**, *29*, 3793−3799.
(59) Liu, M.; Voznyy, O.; Sabatini, R.; Garcia de Arquer, F. P.; Munir, R.; Balawi, A. H.; Lan, X.; Fan, F.; Walters, G.; Kirmani, A. R.; Hoogland, S.; Laquai, F.; Amassian, A.; Sargent, E. H. Hybrid Organic-Inorganic Inks Flatten the Energy Landscape in Colloidal Quantum Dot Solids. *Nat. Mater.* **2017**, *16*, 258−263.
(60) Chuang, C.-H. M.; Brown, P. R.; Bulović, V.; Bawendi, M. G. Improved Performance and Stability in Quantum Dot Solar Cells Through Band Alignment Engineering. *Nat. Mater.* **2014**, *13*, 796−801.

DOI: 10.1021/acscentsci.8b00386
ACS Cent. Sci. 2018, 4, 1352−1359